Journal of Nuclear Materials 389 (2009) 394–401

Contents lists available at ScienceDirect

Journal of Nuclear Materials

journal homepage: www.elsevier.com/locate/jnucmat

Estimation of equilibrium surface precipitation constants for trivalent metal sorption onto hydrous ferric oxide and calcite

Anpalaki J. Ragavan [a,*], Dean V. Adams [b]

[a] Department of Civil and Environmental Engineering, MS258, University of Nevada, Reno, 1215, Beech street, Apt. 26, Reno, NV 89512, USA
[b] College of Engineering, MS 256, University of Nevada, Reno, NV 89557, USA

ARTICLE INFO

Article history:
Received 2 March 2008
Accepted 8 February 2009

PACS:
05.70.−a
05.70.Ce
05.70.Fh
05.70.Np
06.20.Jr
05.60.−k

ABSTRACT

Equilibrium constants for modeling surface precipitation of trivalent metal cations (M^{3+}) onto hydrous ferric oxide and calcite were estimated from linear correlations of standard state Gibbs free energies of formation, ($\Delta G^0_{f,MvX(ss)}$) of the surface precipitates. The surface precipitation reactions were derived from Farley et. al. [K.J. Farley, D.A. Dzombak, F.M.M. Morel, J. Colloid Interface Sci. 106 (1985) 226] surface precipitation model, which are based on surface complexation model coupled with solid solution representation for surface precipitation on the solid surface. The $\Delta G^0_{f,MvX(ss)}$ values were correlated through the following linear free energy relations $\Delta G^0_{f,M(OH)_3(ss)} - 791.70 r_{M^{3+}} = 0.1587\Delta G^0_{n,M^{3+}} - 1273.07$ and $\Delta G^0_{f,M_2(CO_3)_3(ss)} - 197.241 r_{M^{3+}} = 0.278\Delta G^0_{n,M^{3+}} - 1431.27$ where 'ss' stands for the end-member solid component of surface precipitate, $\Delta G^0_{f,MvX(ss)}$ is in kJ/mol, $r_{M^{3+}}$ is the Shannon-Prewitt radius of M^{3+} in a given coordination state (nm), and $\Delta G^0_{n,M^{3+}}$ is the non-solvation contribution to the Gibbs free energy of formation of the aqueous M^{3+} ion. Results indicate that the above surface precipitation correlations are useful tools where experimental data are not available.

1. Introduction

Over the past few years there has been an increasing awareness of the problems associated with the disposal of radioactive waste containing actinides. Research on this problem is spreading over to the lanthanides. The concept of isomorphous substitution is often used to separate radioactive elements. For example, uranium ore also contains very small quantities of radium. To separate the radium, an anion that forms an insoluble compound with the alkaline earth (radium) ion, but which forms soluble compounds with uranium and other actinides can be used. This process is known as surface precipitation (also known as co-precipitation) in the form of solid solutions. Many lanthanides and actinides have been found to migrate from the waste matrix and co-precipitate with other secondary minerals to form thermodynamically stable solid solutions. Surface precipitation onto the surface of solids is therefore a potential way of separating, removing and utilizing the actinides from these waste stockpiles. Surface precipitation of radionuclides with secondary solids is currently thought to be important process limiting radionuclide solution concentrations. The actinides are radioactive, long-lived, and highly toxic.

Over the last few decades, vast quantities of transuranic actinides (those with atomic numbers greater than that of uranium) have been produced inside the fuel rods of commercial nuclear reactors. Currently, most spent fuel rods are stored aboveground in interim storage facilities, but the plan in the United States and some European countries is to deposit this nuclear waste in repositories buried hundreds of meters underground, where surface precipitation and redox reactions determine the species' distribution and stability. Radionuclides such as uranium, neptunium, plutonium, and americium are the major contributors to the long-term radioactivity of nuclear waste currently targeted for the proposed Yucca Mountain repository in Nevada.

On the other hand the concentrations of the actinides in natural waters are typically on the order of 10^{-6} molar (M) or lower [1]. While those concentrations are high enough to be of environmental concern, they are too low to allow direct study with conventional spectroscopies, but require advanced spectroscopic techniques, such as X-ray absorption fine structure (XAFS) and laser-induced fluorescence spectroscopies. Most actinides have fairly short half-lives, synthesized artificially and have limited thermodynamic data available. The exceedingly short half-lives of members of the latter half of the actinide series makes it not feasible to investigate their chemistry. In addition, experimental works using some actinide (e.g., Am) are usually restricted, because special care is required to handle actinide-emitters. The availability of data for lanthanides allows lanthanides to replace actinides as useful predictors of the chemical and thermodynamic properties of actinides. A suitable

Abbreviations: HFO, Hydrous Ferric Oxide; XAFS, X-ray Absorption Fine Structure; EXAFS, Extended XAFS; CN, Coordination Number; PC, Partition Coefficient.

* Corresponding author. Tel.: +1 775 322 3694.
E-mail address: ragavan@unr.edu (A.J. Ragavan).

0022-3115/$ - see front matter © 2009 Elsevier B.V. All rights reserved.
doi:10.1016/j.jnucmat.2009.02.015

lanthanide element is usually allowed to substitute for these actinides. In many ways, the chemical properties of several actinides repeat those of lanthanides. The heavy elements do resemble the lanthanides very closely and the known chemistry of the lanthanides proves invaluable in predicting the chemistry of the actinides. Comparison of the energy characteristics of valence orbital data of actinides and lanthanides demonstrate similarity between the stabilities of trivalent cationic (M^{3+}) species of the first half of the lanthanide series to those of the second half of the actinide [2]. Like the lanthanides, formation of the 3+ ion of actinides corresponds to the loss of the *s* and *d* orbital electrons before those of the *f* orbital electrons.

1.1. Applicability of hydrous ferric oxide and calcite

The crystalline hydroxide phases of iron ($Fe(OH)_3$), and calcite ($CaCO_3$) are useful and increasingly being considered for radionuclide waste removal. $Fe(OH)_3$, is an excellent scavenger of trivalent lanthanides (lanthanum (La) to lutetium (Lu)) and actinides (actinium (Ac) through lawrencium (Lw)) in aqueous solutions. $Fe(OH)_3$ most often forms bidentate surface complexes with trivalent lanthanides and actinides with high coordination numbers that reduce their toxicity. $CaCO_3$, a common secondary mineral found in abundance in fractures and pore fillings, in the earth, has been shown to immobilize trivalent actinides and lanthanides in natural environment in several studies [3–7]. Natural calcite has been shown to incorporate the whole lanthanide series at significant concentrations (4.72 mmol/kg calcite or 4.72×10^{-4} mol fraction) [5]. The highest immobilizations occurred near radioactive waste disposal sites. This indicates that calcite could be important in the removal of actinide bearing radioactive waste. Although "actinides" refers to the fifteen elements with atomic numbers 89 through 103 (actinium through lawrencium), in this paper this term is limited to refer only to uranium, neptunium, plutonium, americium, and curium. These five actinides are the only ones that pose significant environmental concerns [1].

1.2. Currently available modeling approaches

The thermodynamic construct for the continuum between surface complexation and bulk solid precipitation of cations by Farley et. al. [8] suggests that, as a solid surface is loaded with sorbed cations, for example, trivalent metal cation (M^{3+}) onto Hydrous Ferric Oxide Surfaces (HFO, with a nominal formula of $Fe(OH)_3$; [9]), a surface precipitate is formed as a solid solution in the form of $Fe(OH)_3 - M(OH)_3$. With the increase of sorbate/sorbent ratios, both metal surface complexes and the mole fractions of $M(OH)_3$ solid increases until all surface sites become saturated. At this point, surface precipitation becomes the dominant sorption mechanism. Sorption refers to all processes (adsorption or surface complexation, surface precipitation, bulk precipitation, and ion exchange) that transfer an ion from the aqueous phase to the solid phase [10]. The Farley et. al. [8] construct further states that at low sorbate/sorbent ratios (<0.1) the activity of the metal hydroxide phase remains lower, allowing solubility product for onset of surface precipitation of the metal hydroxide to remain far lower, than that required for bulk solid precipitation. Because of the far lower solubility of the solid solution component, $M(OH)_3(ss)$ than that of the bulk solid precipitate, $M(OH)_3$ surface precipitation starts at an aqueous M^{3+} concentration much lower than that required for the precipitation of bulk $M(OH)_3(s)$. With increasing aqueous M^{3+} ion concentrations saturation with respect to bulk $M(OH)_3$ is approached. Precipitation constants of the "fictitious" pure solid solution phases ($M(OH)_3(ss)$) are difficult to obtain experimentally.

The surface precipitation model of Farley et. al. [8] has been applied and found useful to describe sorption data for several divalent and trivalent cations over a wide range of free sorbate concentrations, including the application at high sorbate/sorbent ratios of Zn^{2+}, Pb^{2+},Cd^{2+}, Hg^{2+}, Cr^{3+}, and Cu^{2+} onto hydrous ferric oxide surfaces (HFO) [8,11,9,12,13]; of Zn^{2+}, Mn^{2+}, Cd^{2+} and Co^{2+} sorption onto calcite [14]; of Am^{3+} and Eu^{3+} sorption onto γ-Alumina [15]; of trivalent lanthanides and actinides onto goethite and calcite [16]; and of Co^{2+} sorption onto-alpha-Al_2O_3 [17]. Spectroscopic evidence for the formation of surface precipitates onto HFO, as well as the sorption mechanisms were recently reviewed by several other researchers [17–19]. The subject of surface precipitation is an area of active research. Applications of the Farley et. al. [8] surface precipitation model for trivalent cations are currently limited due to the lack of experimentally derived equilibrium constants for the formation of solid solutions of trivalent cations. Reliable thermodynamic data available in the literature for the surface precipitation of lanthanides and actinides are especially limited.

On the other hand, Sverjensky and Molling [20] proposed an empirical linear free energy correlation for crystalline solids of divalent cations. The linear free energy formula of Sverjensky and Molling [20] is analogous to the well-known Hammett relationship developed for functional group substitution in organic compounds [21,22]. The Sverjensky and Molling [20] correlation has been successfully applied to various crystalline structure families of divalent and tetravalent cations to predict surface reaction controlled dissolution rates and formation energies of end-members [23–28]. This linear free energy equation quantifies cation substitution in crystalline solids hence can be used to predict the rates at which solids react [20].

In this paper the Farley et al. [8] surface precipitation model along with linear free energy relations, were evaluated as a theoretical construct for the estimation of equilibrium constants for surface precipitation of trivalent lanthanides and actinides onto HFO and calcite.

2. Model adaptation for present work

The original Sverjensky and Molling [20] linear free energy relationship was modified to be applied to derive standard state Gibbs free energies of formation ($\Delta G^0_{f,MvX(ss)}$) of surface precipitates with HFO and calcite structure. The modified Sverjensky and Molling [20] equation for trivalent cations is given as:

$$\Delta G^0_{f,MvX} - \beta_{MvX} r_{M^{3+}} = a_{MvX} \Delta G^0_{n,M^{3+}} + b_{MvX} \quad (1)$$

where $\Delta G^0_{f,MvX}$ denotes the standard state Gibbs free energies of formation of end-member solids (MvX) in the solid solution (surface precipitate), $r_{M^{3+}}$ represents the Shannon-Prewitt radius [29] of the M^{3+} cation in a given coordination state, and $\Delta G^0_{n,M^{3+}}$ denotes the non-solvation contribution to the Gibbs free energy of formation of the aqueous M^{3+} ion. The coefficients a_{MvX}, b_{MvX}, and β_{MvX} are regression parameters. Values of coefficient a_{MvX} are related only to the stoichiometry of the crystal solid formed and are very close for all polymorphs of the composition MvX [20]. The coefficient β_{MvX} is only related to the effect of nearest neighbors of the cation (or coordination numbers: CN) in the solid formed. In polymorphs, the structure family with small CN (e.g., CN = 6 in calcite structure family) has higher value of β_{MvX} than does the family with large CN (e.g., CN = 9 in aragonite structure family) [20]. The coefficient b_{MvX} reflects characteristic of the reaction type and conditions under which solid solution formation took place regardless of the valence of the cation or the stoichiometry of the solid.

Although Eq. (1) applies to the free energies of crystalline solids, it was initially developed as a family of linear free energy equations for aqueous and mixed solvent organic reactions [21,22]. One of these is the Hammett equation, which has the form:

$$Log(K/K_0) = \sigma\rho \quad (2)$$

where K and K_0 represent the equilibrium (or rate) constants for substituted and unsubstituted reactions involving a series of substituent functional group. Each substituent functional group has a characteristic group σ. ρ is a regression coefficient characteristic of the reaction conditions. The substituent parameter σ is derived from equilibrium constants of substituted (K^b) and unsubstituted (K_0^b) species of the functional group according to the equation:

$$\sigma = Log(K_b/K_0^b) \tag{3}$$

The relationship of Eq. (1) to the Hammett equation can be established by converting Eq. (1) to equilibrium constants and by including a reference reaction for a specific cation (N) as follows:

$$Log(K_{MvX}/K_{NvX}) = \sigma_{M^{3+}}\rho_{MvX} + \beta_{MvX}r^* \tag{4}$$

where

$$\sigma_{M^{3+}} = Log(K_{M^{3+}}/K_{N^{3+}}) \tag{5}$$

$$\rho_{MvX} = a_{MvX} \tag{6}$$

and

$$r^* = -(r_{M^{3+}} - r_{N^{3+}})/2.303RT \tag{7}$$

Addition of $\beta_{MvX}r^*$ in Eq. (4) enables the application of Eq. (4) accurately to crystalline solids. The success of Eq. (1) in describing the standard state Gibbs free energies of formation of numerous isostructural families of crystalline solids [20,30], and the analogy with the Hammett equation as described above, suggests that the linear free energy relation for crystalline solids might be applicable to the rate at which solids react. Hence we explored the possibility of applying the linear free energy relation for calculating surface precipitation constants of isostructural families of trivalent metal hydroxides and calcite respectively for which no reliable thermodynamic data are currently available.

According to the hypothesis of surface reaction control and transition state theory, rate of reaction (r') for hydroxides and carbonates far from equilibrium can be related to the rate constant (k) by the following equation:

$$\log(r') = \log(k) + n\log(a_{H^+}^c) \tag{8}$$

where $a_{H^+}^c$ represents the activity of aqueous H^+ ions and n the order of the reaction [31]. Experimental surface reaction controlled dissolution rates have been discussed in Casey and Westrich [32] in detail. For constant n (n is roughly constant for each structure), it is possible to develop linear free energy relations involving the function $2.303RT\log(r')$.

One such relation employs involving the trivalent cation parameters $\Delta G^0_{n,M^{3+}}$ and $r_{M^{3+}}$ as:

$$2.303RT\log(r') + \beta r_{M^{3+}} = a'\Delta G^0_{n,M^{3+}} + b' \tag{9}$$

Eq. (9) yields strong linear free energy correlations, using the β values defined by the regression of the standard state Gibbs free energies. The standard state free energy of reaction ($\Delta G^0_{R,MvX(ss)}$) forming a surface precipitate on a surface of a solid as a solid solution can be defined by:

$$\Delta G^0_{R,MvX(ss)} = -2.303RT\log(r') \tag{10}$$

Thus the linear free energy correlation of Sverjensky and Molling [20] permits the prediction of the equilibrium constants of the surface precipitation reactions.

2.1. Standard state Gibbs free energy of surface precipitation reactions

The standard state Gibbs free energy of formation of the end-member of the solid solution on the surface of the solid can be defined as follows (derivation of Eq. (11) for HFO and calcite are given below in Sections 3.1 and 3.2, respectively):

$$\Delta G^0_{f,MvX(ss)} = \Delta G^0_{R,MvX(ss)} + \Delta G^0_{f,M^{3+}} + 3\Delta G^0_{f,H_2O} - 3\Delta G^0_{f,H^+} \tag{11}$$

where $\Delta G^0_{f,MvX(ss)}$ is the standard state Gibbs free energy of formation of the pure end-member component of the solid solution with MvX structure. The $\Delta G^0_{f,M^{3+}}$, $\Delta G^0_{f,H^+}$, and $\Delta G^0_{f,H_2O}$ are the conventional apparent free energy of formation of the trivalent cation, hydrogen ion and water. Definition of the empirical standard state Gibbs free energy of formation of the end-member component of solid solution permits the most direct analogy to Eq. (1) described through the following linear relation:

$$\Delta G^0_{f,MvX(ss)} - \beta'_{MvX}r_{M^{3+}} = a'_{MvX}\Delta G^0_{n,M^{3+}} + b'_{MvX} \tag{12}$$

The regression parameters $\beta'_{MvX}, a'_{MvX}, b'_{MvX}$ are analogous to regression parameters ($\beta_{MvX}, a_{MvX}, b_{MvX}$) of the bulk solid precipitates in Eq. (1). Since the end-member components of the surface precipitates and the bulk precipitates are polymorphs with stoichiometry equal to MvX, the regression parameters a_{MvX} and a'_{MvX} are similar or very close to each other [20]. In addition since the end-member components of the surface precipitates and the bulk solid precipitates possess the same crystal structure (calcite or HFO), hence have same cationic CN in the solids. Therefore, the regression coefficients β_{MvX} and β'_{MvX} are similar [20]. The regression coefficients a_{MvX}, β_{MvX} obtained through regressing the standard state Gibbs free energies of formation of bulk solid precipitates through Eq. (1) can be used to develop linear free energy correlations for the end-member components of the solid solutions with same crystal structures (HFO or calcite).

In this study the standard state, Gibbs free energies of formation of the end-member solids of solid solutions ($\Delta G^0_{f,MvX(ss)}$) with HFO and calcite structures were calculated using the regression coefficients (a_{MvX} and β_{MvX}) obtained from the regression relation developed for the bulk solid precipitates. The regression coefficient b'_{MvX} for this free energy relation was obtained from similar free energy equations developed for the solid solution formation in surface precipitation reactions of divalent cations onto HFO and calcite by Zhu [33] under similar reaction conditions. The regression coefficient b'_{MvX} depends only on reaction type [20]. According to Sverjensky [30] within experimental uncertainties the same regression parameters apply to pure solids formed by bulk precipitation as well as for the pure "fictitious" end-members of the solid solution of polymorphic crystalline structure.

The $\Delta G^0_{R,MvX(ss)}$ values for surface precipitates were calculated from the empirical correlations (Eq. (11)) and were used to estimate the equilibrium constants for surface precipitation reactions onto calcite and HFO, for the following trivalent cations: Dy^{3+},Er^{3+},Tm^{3+}, Lu^{3+}, Ho^{3+}, La^{3+}, Nd^{3+}, Ce^{3+}, Pr^{3+}, Gd^{3+}, Sm^{3+}, Tb^{3+}, Yb^{3+}, Y^{3+}, Eu^{3+}, Am^{3+}, Np^{3+}, U^{3+}, and Pu^{3+}, for which reliable experimental thermodynamic data are currently not available. The surface precipitation reactions were formulated based on the Farley et. al. [8] solid solution model linked to the surface complexation model of Dzobmbak and Morel [9]. The calculated surface precipitation constants need to be verified against experimentally derived surface precipitation constants. Applicability of the model to individual metal ions due to differences of ionic radius and other ionic properties also need to be tested experimentally for respective individual cations.

3. Model development

3.1. Surface precipitation onto HFO

Surface precipitation reactions of trivalent cations onto hydrous ferric oxide can be defined following Farley et. al. [8], Dzombak and Morel [9] and Stumm [5] as follows

$$\equiv FeOH^0 + M^{3+} + 3H_20 \Longleftrightarrow Fe(OH)_3(ss) + =MOH^0 + 3H^+ \quad (13)$$

where the subscript 'ss' stands for the end-member component of the solid solution $Fe(OH)_3 - M(OH)_3$, symbol '≡' (triple) and '=' (double) denote the bonds of metal atoms at the solid surface. The $\equiv FeOH^0$ represents concentrations of $Fe(OH)_3$ surface sites and $=MOH^0$ represents the concentrations of $M(OH)_3$ surface sites [8]. The $\Longleftrightarrow$ sign was used to indicate equality. At high surface coverage the sorption of M^{3+} and Fe^{3+} onto the sorbent surface forms a solid solution of $Fe(OH)_3 - M(OH)_3$ [8,9] as shown below.

$$=MOH^0 + M^{3+} + 3H_2O \Longleftrightarrow M(OH)_3(ss) + =MOH^0 + 3H^+ \quad (14)$$

$$\equiv FeOH^0 + Fe^{3+} + 3H_2O \Longleftrightarrow Fe(OH)_3(ss) + \equiv FeOH^0 + 3H^+ \quad (15)$$

The components of the solid solution obey the mass balance constraint as:

$$X_{Fe(OH)_3(ss)} + X_{M(OH)_3(ss)} = 1 \quad (16)$$

where X stands for the mole fraction of an end-member component in the solid solution and are calculated from:

$$X_{M(OH)_3(ss)} = \frac{[M(OH)_3(ss)]}{[M(OH)_3(ss)] + [Fe(OH)_3(ss)]} \quad (17)$$

$$X_{Fe(OH)_3(ss)} = \frac{[Fe(OH)_3(ss)]}{[M(OH)_3(ss)] + [Fe(OH)_3(ss)]} \quad (18)$$

where the brackets, [], stand for the mole concentrations of components per liter of aqueous solution.

For an ideal solid solution, the activity of the component 'i' (a_i^{aq}) in the solid solution is equal to X_i. Most $M(OH)_3$ solid (pure end-members and bulk solids) have a structure similar to HFO. In addition the substitution is isovalent, for most applications. Hence mixing in this type of solid solution can be considered ideal. As a result, the activity coefficients for both $Fe(OH)_3(ss)$ and the end-member $M(OH)_3(ss)$ are unity in the dilute solution regions where Henry's law is obeyed for the $M(OH)_3(ss)$ component [34]. Henrian standard state for $M(OH)_3(ss)$ assumes a hypothetical pure $M(OH)_3(ss)$ end-member of the solid solution with an HFO structure. In such systems the mole balance equation for modeling surface precipitation can be described by the following construct [8,9].

$$TOTM \Longleftrightarrow \sum [M^{3+}]_{aq} + [MOH^0] + [M(OH)_3(ss)] \quad (19)$$

$$TOTFe \Longleftrightarrow \sum [Fe^{3+}]_{aq} + ([FeOH^0] - [MOH^0]) + [Fe(OH)_3(ss)] \quad (20)$$

$$TOT(\equiv FeOH) \Longleftrightarrow [\equiv FeOH^0] + [\equiv FeOH_2^+] + [\equiv FeO^-] + [MOH^0] \quad (21)$$

$$TOTH \Longleftrightarrow [H^+] - [OH^-] + [MOH^{2+}] + 2[M(OH)_2^+] + [\equiv FeOH_2^+] - [\equiv FeO^-] + 2[=MOH^0] - 3[M(OH)_3(ss)] - 3[Fe(OH)_3(ss)] \quad (22)$$

where the symbols $TOTM, TOTFe, TOT(\equiv FeOH)$, and $TOTH$ denote the total concentrations computed with $M^{3+}, Fe^{3+}, \equiv FeOH$, and H^+ as components in the system in a tableau representation of the system. The summation sign stands for the sum of all aqueous species and complexes of M^{3+} or Fe^{3+} ion and $\equiv FeOH$ stands for surface site. Following the assumption of Farley et al. [8] and Dzombak and Morel [9], all precipitated Fe is accounted for in the calculation of mole fractions in Eqs. (17) and (18).

3.2. Surface precipitation onto calcite

The reaction of M^{3+} precipitation onto calcite can be written as:

$$=CaCO_3^0 + M^{3+} + HCO_3^- \Longleftrightarrow CaCO_3(ss) + =MCO_3^+ + H^+ \quad (23)$$

The solid solution formation of M^{3+} and Ca^{2+} onto the sorbent surface is given as:

$$=MCO_3^+ + 2M^{3+} + 3HCO_3^- \Longleftrightarrow M_2(CO_3)_3(ss) + =MCO_3^+ + 3H^+ \quad (24)$$

$$=CaCO_3^0 + Ca^{2+} + HCO_3^- \Longleftrightarrow CaCO_3(ss) + =CaCO_3^0 + H^+ \quad (25)$$

The mass balance constraints require:

$$TOTM \Longleftrightarrow \sum [M^{3+}]_{(aq)} + [=MCO_3^+] + [M_2(CO_3)_3(ss)] \quad (26)$$

$$TOTCa \Longleftrightarrow \sum [Ca^{2+}]_{(aq)} + [=CaCO_3^0] + [CaCO_3(ss)] \quad (27)$$

$$TOT(=CaCO_3) \Longleftrightarrow [=CaCO_3^0] + [=MCO_3^+] \quad (28)$$

In this case the substitution is non iso-valent and the $M_2(CO_3)_3$ solids have a different structure from $CaCO_3$. The mixing in this type of solid solution is most likely non ideal [18]. However, assuming an ideal solid solution is reasonable for most applications, as long as Henrian standard state for the $M_2(CO_3)_3$ end-member of the precipitation is defined. A Raoultian standard state was assumed for the $CaCO_3$ end-member which defines unit activity for this end-member component. Henrian standard state defines unit activity for the hypothetical $M_2(CO_3)_3$ end-member of the solid solution with a calcite structure extrapolated along the Henry's law slope from the infinitely dilute solution regions. According to the above definitions, the activity coefficients of both $CaCO_3$ and $M_2(CO_3)_3$ end-members are unity in the dilute solutions regions where Henry's law is obeyed for $M_2(CO_3)_3$ component [33–35]. This assumption is reasonable since total Gibbs energy is independent of the choice of the standard state and the solid solution components are produced in trace amounts.

3.3. Equilibrium surface precipitation constants

The standard Gibbs free energies of formation for the pure bulk $M(OH)_3(s)$ solids with HFO structure and pure bulk $M_2(CO_3)_3$ solids with calcite structure were obtained through the Sverjensky and Molling [20] equation modified for trivalent cations (Eq. (1)). The regression coefficients obtained from this correlation were used to calculate the standard state Gibbs free energies of formation of the "fictitious" pure end-members of the solid solutions onto HFO and calcite as described in the introduction. From the standard state Gibbs free energies of formation of the 'fictitious' pure end-members of the solid solution the standard state Gibbs free energies of reactions of the solid solution onto HFO and calcite were calculated as:

$$\Delta G^0_{R,M(OH)_3(ss)} = \Delta G^0_{f,M(OH)_3(ss)} - \Delta G^0_{f,M^{3+}} - 3\Delta G^0_{f,H_2O} + 3\Delta G^0_{f,H^+} \quad (29)$$

$$\Delta G^0_{R,M_2(CO_3)_3(ss)} = \Delta G^0_{f,M_2(CO_3)_3(ss)} - 2\Delta G^0_{f,M^{3+}} - 3\Delta G^0_{f,HCO_3^-} + 3\Delta G^0_{f,H^+} \quad (30)$$

where $\Delta G^0_{f,M(OH)_3(ss)}$ is the standard state Gibbs free energy of formation of the $M(OH)_3$ end-member component of the solid solution onto HFO, $\Delta G^0_{f,M_2(CO_3)_3(ss)}$ is that of the $M_2(CO_3)_3$ end-member component of the solid solution onto calcite. $\Delta G^0_{R,M\nu X(ss)}$ is the standard state Gibbs free energy of the solid solution reaction for the solid ($M\nu X$) with HFO or calcite structures ($M(OH)_3$ or $M_2(CO_3)_3$). The thermodynamic construct of derivation of Eq. (29) and Eq. (30) are given above in Sections 3.1 and 3.2 respectively.

A standard state unit activity of pure water was assumed for water. For aqueous species other than water, unit activity of the species in a hypothetical one molal ideal solution referenced to infinite dilution at the temperature and pressure of interest defines the standard state. The standard state Gibbs free energies of formation

of water and bicarbonates were obtained from Shock and Helgeson [36]. Values of ΔG_f^o of the cations are from Brookins [37].

Finally the equilibrium solubility products (K) for the solid solution reactions were calculated using the standard state Gibbs free energies of the solid solution reactions as:

$$\Delta G^0_{R,M\nu X(ss)} = -2.303RT\ln(K) \quad (31)$$

where K are the values of the equilibrium constants for reactions given in Eq. (14), and Eq. (24), R is the gas constant and T is the temperature in Kelvin. The K values thus calculated are the solubility products of the pure end-member components of the solid solution with HFO or calcite structure.

4. Results

The following linear free energy correlations were obtained for the pure bulk solid precipitates by performing a multiple linear regression analysis using experimental standard state Gibbs free energies of formation and trivalent cation parameters listed in Table 1 (HFO structure) and Table 2 (calcite structure), based on Eq. (1).on HFO:

$$\Delta G^0_{f,M(OH)_3(s)} - 791.70 r_{M^{3+}} = 0.159\Delta G^0_{n,M^{3+}} - 1474.09 \quad (32)$$

and on calcite:

$$\Delta G^0_{f,M_2(CO_3)_3(s)} - 197.241 r_{M^{3+}} = 0.278\Delta G^0_{n,M^{3+}} - 3325.75 \quad (33)$$

Figs. 1a and 2a show this regression results respectively for the HFO and calcite structures. Correlations are statistically significant at the 5% significance level (R^2 = 0.99, and R^2 = 0.96 respectively for HFO and calcite, see Table 3). The standard state Gibbs free energies of formation of the bulk solid precipitate calculated from the above correlations are shown in Table 1 and Table 2 (column 6) for HFO and calcite structures respectively. The deviations of the calculated values obtained from Eq. (32) for HFO and Eq. (33) for calcite from the experimental values of the Gibbs free energies of formation of the bulk solids were within ±2.0% for HFO structure and within ±1.75% for calcite structure (Figs. 1b and 2b). Discrepancies are larger for the hydroxide structure family than for the calcite structure family. Developed relationship support the fact that, most $M_2(CO_3)_3$ (s) have calcite structure and all $M(OH)_3(s)$ have HFO structure [33]. The discrepancies between the calculated and the experimental Gibbs free energies are acceptable considering the metastable nature of the solids. These correlations from Eq. (32) and Eq. (33) allow prediction of standard state Gibbs free energies of formation of the pure end-members of solid solution, and the equilibrium constants for solid solution reactions for which there are no reliable experimental data currently available.

The following regression correlations were developed for the Gibbs free energies of formation of the pure end-member components of the solid solutions, using the coefficients $a_{M\nu X}, \beta_{M\nu X}$ obtained from the correlations developed for the bulk solids with HFO structure (Eq. (32)) and calcite structure (Eq. (33)), and the coefficient $b_{M\nu X}$ obtained from Zhu [34] for the surface precipitation of divalent cations onto HFO and calcite under similar reaction conditions.on HFO:

$$\Delta G^0_{f,M(OH)_3(ss)} - 791.70 r_{M^{3+}} = 0.159\Delta G^0_{n,M^{3+}} - 1273.07 \quad (34)$$

on calcite:

$$\Delta G^0_{f,M_2(CO_3)_3(ss)} - 197.241 r_{M^{3+}} = 0.278\Delta G^0_{n,M^{3+}} - 1431.27 \quad (35)$$

The standard state Gibbs free energies of formation of the pure end-members of the solid solution with HFO and calcite structures obtained respectively using Eq. (34) and Eq. (35) are given in Table 1 and Table 2 respectively (column 7). The $\Delta G^0_{R,M\nu X(ss)}$ values calculated from Eq. (29) and Eq. (30) for the solid solution reactions for HFO and calcite respectively (column 8) and the equilibrium surface precipitation constants (column 9) calculated from Eq. (31) for the respective solid end-members are listed in Table 1 and Table 2, respectively. The equilibrium constants (solubility products) of the bulk $M(OH)_3(s)$ and $M_2(CO_3)_3(s)$ solid precipitates were also calculated in similar way using the standard state Gibbs free energies of formation of pure bulk solids in Eq. (29) and Eq. (30) for the respective solids and the equilibrium constants calculated from Eq. (31). The equilibrium constants of the bulk solid precipitation reactions thus calculated are shown in column 10 of Table 1 (for HFO structure) and Table 2 (for calcite structure) for comparison.

The equilibrium constants for the solid solution reactions were much smaller than that of the bulk solid precipitation reactions

Table 1
Experimental and calculated thermodynamic data for pure bulk and solid solution $M(OH)_3$ component solid.

M^{3+}	$r_{M^{3+}}$ (nm)	$\Delta G^o_{f,M^{3+}}$ (kJ/mol)	$\Delta G^o_{n,M^{3+}}$ (kJ/mol)	$\Delta G^o_{f,M(OH)_3(s)}$ Experimental (kJ/mol)	$\Delta G^o_{f,M(OH)_3(s)}$ Calculated (kJ/mol)	$\Delta G^o_{f,M(OH)_3(ss)}$ Calculated (kJ/mol)	$\Delta G^o_{R,M(OH)_3(ss)}$ Calculated (kJ/mol)	$Log(K)$ Calculated $M(OH)_{3(ss)}$	$Log(K)$ Calculated $M(OH)_{3(s)}$
Dy^{3+}	0.0908	−665.70	787.21	−1286.18	−1279.79	−1078.77	295.90	−51.86	−16.63
Er^{3+}	0.0881	−669.47	785.41	−1295.81	−1279.41	−1078.39	300.04	−52.58	−17.35
Tm^{3+}	0.087	−662.35	793.33	−1288.70	−1279.96	−1078.94	292.37	−51.24	−16.01
Lu^{3+}	0.085	−628.02	829.12	−1257.30	−1283.03	−1082.01	254.97	−44.68	−9.45
Ho^{3+}	0.0894	−674.07	779.85	−1298.33	−1271.73	−1070.71	312.33	−54.74	−19.51
La^{3+}	0.1061	−684.12	757.70	−1280.32	−1267.16	−1066.14	326.95	−57.30	−22.07
Nd^{3+}	0.0995	−671.98	774.61	−1277.81	−1273.79	−1072.77	308.18	−54.01	−18.78
Ce^{3+}	0.1034	−672.40	771.37	−1271.11	−1268.14	−1067.12	314.24	−55.07	−19.84
Pr^{3+}	0.1013	−679.52	765.77	−1285.77	−1267.01	−1065.99	322.49	−56.52	−21.29
Gd^{3+}	0.0938	−661.51	789.21	−1284.93	−1273.93	−1072.91	297.57	−52.15	−16.92
Sm^{3+}	0.0964	−666.96	781.88	−1284.93	−1269.71	−1068.69	307.23	−53.84	−18.61
Tb^{3+}	0.0923	−652.30	799.51	−1270.28	−1248.95	−1047.93	313.34	−54.91	−19.68
Yb^{3+}	0.093	−644.35	806.96	−1272.37	−1254.21	−1053.19	300.12	−52.60	−17.37
Eu^{3+}	0.095	−574.43	875.42	–	−1274.23	−1073.21	210.18	−36.83	−1.60
Am^{3+}	0.107	−599.51	841.66	–	−1269.13	−1068.11	240.36	−42.12	−6.89
Np^{3+}	0.110	−517.45	921.57	–	−1248.07	−1047.05	179.36	−31.43	3.80
U^{3+}	0.1165	−476.50	957.85	–	−1245.05	−1044.03	141.43	−24.79	10.44
Pu^{3+}	0.108	−578.41	862.05	–	−1255.01	−1053.99	233.38	−40.90	−5.67

Cationic radii are from Refs. [29,36]. Values of ΔG_f^o of the cations are from Ref. [37]. The values of the experimental $\Delta G^o_{f(s)}$ of the bulk precipitate solid crystals are from Ref. [37]. The calculated $\Delta G^o_{f(s)}$ values of the bulk precipitate solid crystals are from Eq. (1). Calculated $\Delta G^o_{R(ss)}$ and $\Delta G^o_{f(ss)}$ values of the solid solution component are from Eq. (29) and Eq. (34). Calculated Log K values for the solid reactions (column 9 from left) and the bulk precipitation (column 10 from left) are from Eq. (31) using the $\Delta G^o_{f(ss)}$ of the component of the solid solution (column 7 from left) and that of bulk precipitate (column 6 from left). All calculations are at 25 °C and 1 bar.

Table 2
Experimental and calculated thermodynamic data for pure bulk and solid solution $M_2(CO_3)_3$ component solid.

M^{3+}	$r_{M^{3+}}$ (nm)	$\Delta G^o_{f,M^{3+}}$ (kJ/mol)	$\Delta G^o_{n,M^{3+}}$ (kJ/mol)	$\Delta G^o_{f,M_2(CO_3)_3(s)}$ Experimental (kJ/mol)	$\Delta G^o_{f,M_2(CO_3)_3(s)}$ Calculated (kJ/mol)	$\Delta G^o_{f,M_2(CO_3)_3(ss)}$ Calculated (kJ/mol)	$\Delta G^o_{R,M_2(CO_3)_3(ss)}$ Calculated (kJ/mol)	$Log(K)$ Calculated $M_2(CO_3)_{3,ss)}$	$Log(K)$ Calculated $M_2(CO_3)_{3(s)}$
Dy^{3+}	0.0908	−665.70	787.21	−3095.30	−3089.00	−1194.52	1898.88	−332.78	−0.77
Er^{3+}	0.0881	−669.47	785.41	−3109.54	−3090.03	−1195.55	1905.39	−333.92	−1.91
Tm^{3+}	0.087	−662.35	793.33	−3095.30	−3088.04	−1193.56	1893.13	−331.77	0.24
Lu^{3+}	0.085	−628.02	829.12	−3026.64	−3078.49	−1184.01	1834.03	−321.41	10.59
Ho^{3+}	0.0894	−674.07	779.85	−3118.75	−3091.32	−1196.84	1913.30	−335.30	−3.30
La^{3+}	0.1061	−684.12	757.7	−3143.87	−3094.18	−1199.70	1930.54	−338.32	−6.32
Nd^{3+}	0.0995	−671.98	774.61	−3104.09	−3090.78	−1196.30	1909.65	−334.66	−2.66
Ce^{3+}	0.1034	−672.40	771.37	−3115.40	−3090.91	−1196.43	1910.36	−334.79	−2.78
Pr^{3+}	0.1013	−679.52	765.77	−3127.96	−3092.89	−1198.41	1922.63	−336.94	−4.93
Gd^{3+}	0.0938	−661.51	789.21	−3093.63	−3087.85	−1193.37	1891.65	−331.51	0.50
Sm^{3+}	0.0964	−666.96	781.88	−3104.09	−3089.37	−1194.89	1901.02	−333.15	−1.15
Tb^{3+}	0.0923	−652.30	799.51	−3075.20	−3085.28	−1190.80	1875.80	−328.73	3.27
Yb^{3+}	0.093	−644.35	806.96	−3052.60	−3083.07	−1188.59	1862.11	−326.33	5.67
Eu^{3+}	0.095	−574.43	875.42	–	−3063.64	−1169.16	1741.69	−305.23	26.77
Am^{3+}	0.107	−599.51	841.66	–	−3070.66	−1176.18	1784.84	−312.79	19.21
Np^{3+}	0.110	−517.45	921.57	–	−3047.86	−1153.38	1643.52	−288.03	43.98
U^{3+}	0.1165	−476.50	957.85	–	−3036.49	−1142.01	1572.99	−275.66	56.34
Pu^{3+}	0.108	−578.41	862.05	–	−3064.80	−1170.32	1748.50	−306.42	25.58

Cationic radii are from Refs. [29,36]. Values of ΔG^o_f of the cations are from Ref. [37]. The values of the experimental $\Delta G^o_{f(s)}$ of the bulk precipitate solid crystals are from Ref.[37]. The calculated $\Delta G^o_{f(s)}$ values of the bulk precipitate solid crystals are from Eq. (1). Calculated $\Delta G^o_{R(ss)}$ and $\Delta G^o_{f(ss)}$ values of the solid solution component are from Eq. (30) and Eq. (35). Calculated Log K values for the solid solution reactions (column 9 from left) and bulk solid precipitation (column 10 from left) are from Eq. (31) using the $\Delta G^o_{f(ss)}$ of the component of the solid solution (column 7 from left) and that of bulk precipitate (column 6 from left). All calculations are at 25 °C and 1 bar.

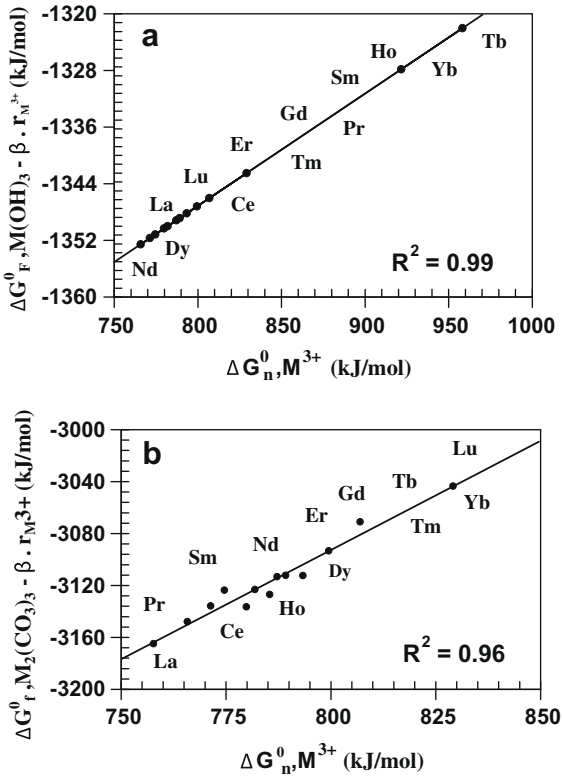

Fig. 1. (a) Multiple linear regression. Graphical representation of Eq. (1) for the standard state Gibbs free energies of formation of the bulk solid trivalent metal hydroxides with HFO structure. Regression calculations were computed using Eq. (1) and using the data from Table 1. The vertical axis shows the left side of Eq. (1). (b) Difference in values between experimentally derived and the calculated standard state Gibbs free energies of formation of the trivalent bulk solid hydroxides from Eq. (1). The experimental values are from Ref. [37].

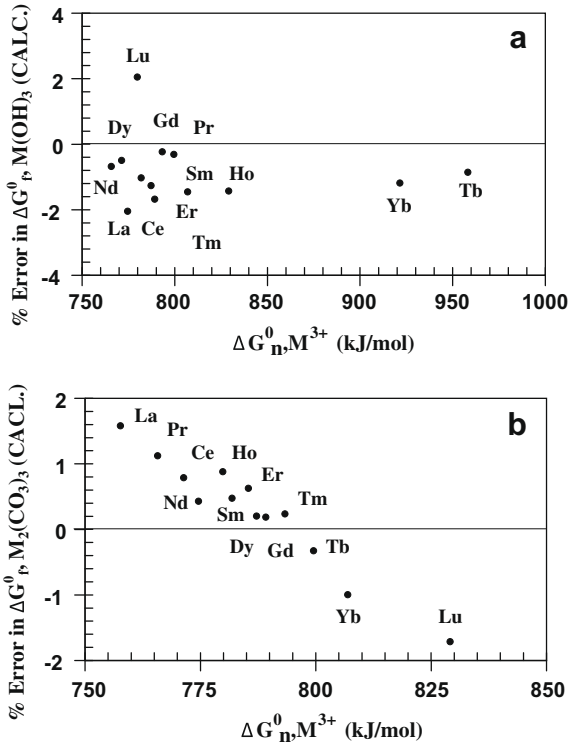

Fig. 2. (a) Multiple linear regression. Graphical representation of Eq. (1) for the standard state Gibbs free energies of formation of the bulk solid trivalent metal carbonates with calcite structure. Regression calculations were computed using Eq. (1) and using data from Table 2. The vertical axis shows the left side of Eq.(1). (b) Difference in values between experimentally derived and calculated standard state Gibbs free energies of formation of the trivalent bulk solid carbonates from Eq. (1). The experimental values are from Ref. [37].

(see columns 9 and 10 for HFO (Table 1) and calcite (Table 2) structures respectively). The results are consistent with the results from previous studies [33,38] as well as with the Farley et. al. [8] surface precipitation model, which states that the solubilities of the solid solution components are far lower than those of the bulk solid precipitates which allow surface precipitation to occur at much lower concentrations of the cations in the solutions than that required for bulk solid precipitation to occur.

Table 3
Summary of regression analysis: Gibbs free energies of formation of bulk solids.

Sorbent	a_{MX}	b_{MX} kJ/mol	β_{MX} kJ/mol nm	R^2
HFO	0.159	−1474.09	791.70	0.99
Calcite	0.278	−3325.75	197.24	0.96

The correlation coefficients are from $\Delta G^0_{f,M\nu X} - \beta_{M\nu X} r_{M^{3+}} = a_{M\nu X}\Delta G^0_{n,M^{3+}} + b_{M\nu X}$. All calculations are at 25 °C and 1 bar.

5. Discussion

Solid solution models are a major approach to quantify surface precipitation processes. Solid solution models are based on the laws of chemical thermodynamics and in principle generally valid. However, the limited availability of thermodynamic data for many radionuclides limits their applicability to radionuclides. This paper provides a useful method to the estimation of equilibrium constants for surface precipitation of trivalent lanthanides and actinides onto HFO and calcite. The high significance of the correlation parameters emphasizes the adequacy of the model.

A single radionuclide may form a variety of solids, each characterized by a particular solubility product. It is difficult to predict which of these solids will effectively precipitate under the conditions of interest. In the III and IV states, actinides form hydrated An^{3+} and An^{4+} ions in solution, respectively. In contrast, the highly charged ions in the V and VI states are unstable in aqueous solution and hydrolyze instantly to form linear *trans*-dioxo cations, AnO_2^+ and AnO_2^{2+}, with overall charges of 1+ and 2+, respectively [1]. Very strong partition of trivalent actinides and lanthanides onto calcite (PC (partition coefficients) between 200 and 1000) has been reported by Curti [38] compared to divalent (PC between <1 and 10) and tetravalent (PC between 20 and 200) cations. The low solubilities of the hydroxide and calcite solids formed by the cations of trivalent lanthanides and actinides compared to that formed by cations of valences other that 3+ facilitate their uptake.

On the other hand, carbonates (CO_3^{2-}) and hydroxides (OH^-) are the two most important ligands found in natural waters. Under the strongly reducing conditions of the ground waters and underground repositories, all actinides species are dominated by the trivalent oxidation states like lanthanides. For example americium and curium will only be found in the 3+ oxidation state under most conditions. All actinides beyond curium are dominated by the lanthanide-like trivalent oxidation state. Trivalent lanthanides and actinides of calcite and hydroxide structure can be expected to be the dominant solid solutions formed under natural environmental conditions, which makes surface precipitation onto these two solids to be major contributors to radioactive waste removal.

The developed model gave larger $\beta_{M\nu X}$ values for solid solutions of trivalent lanthanides and actinides onto HFO (791.7 kJ/mol nm, Table 3) compared to that onto calcite (197.24 kJ/mol nm, Table 3). Zhu [33] too reported slightly larger $\beta_{M\nu X}$ values for surface precipitation of divalent M^{2+} cations including lanthanides and actinides (Eu^{2+}, Ra^{2+}, UO_2^{2+}) onto calcite (83.99 kcal/mol Å) compared to that onto HFO (77.21 kcal/mol Å). This can be attributed to the differences in valences between the metal cations and of the solid cations (Fe^{3+} and Ca^{2+}) which is related to the CN of the metal cations. Valences being equal the affinity of the metal for the calcite and HFO surfaces has been found to depend only on the degree to which the ionic radius of the metal cation matches that of Ca^{2+} and the Fe^{3+} ions [39]. According to Sverjensky [30] the coefficient $\beta_{M\nu X}$ is related to the effect of nearest neighbors or CN of the metal cation. Recent calculations by Bosbach et. al., [40] using extended XAFS (EXAFS) spectroscopic measurements indicate a CN in the order of 7.1 ± 1.1 for trivalent actinides with calcite structure.

The $a_{M\nu X}$ correlation parameter calculated for trivalent cations in the present study were larger compared to the $a_{M\nu X}$ developed for divalent cations with the same structure in previous studies [33] due to the differences in stoichiometry of solid solutions. For divalent cations with an HFO structure a larger value of $a_{M\nu X}$ (1.03266 was reported by Zhu [33], R^2 = 0.99) can be expected compared to the value of 0.1587 calculated in this study for trivalent cations due to smaller OH^-: M^{2+} ratio in $M(OH)_2$ of 2:1 compared to the 3:1 in $M(OH)_3$. Larger $a_{M\nu X}$ value (0.915, R^2 = 0.99, [33]) was also reported for divalent cations with the MCO_3 stoichiometry compared to 0.287 calculated for trivalent cations with the $M_2(CO_3)_3$ stoichiometry in this study.

Development of strong linear free energy correlations was possible because of the fact that the value of n for each structure is roughly constant, which makes Eq. (9) to depend only on the cation parameters and the rate of reaction. The free energy parameter $a_{M\nu X}$ is remarkably close to the dissolution rate parameter [30,33], which is a constant for an isostructural family. The same conditions apply to the parameter $\beta_{M\nu X}$.

In order to apply the linear free energy relationship, the coefficients $a_{M\nu X}$ and $\beta_{M\nu X}$ need to be estimated independently for solids with different stoichiometry and CN.

It should also be mentioned here that the developed surface precipitation model assumes sorption under equilibrium conditions with respect to the solubility of solid, hence independent of kinetic factors. The equilibrium conditions also emphasize that, deviations from non-ideality are insignificant. In addition, trivalent lanthanides and actinides have been reported to form pure anhydrous hydroxides and carbonates, hence to follow the Fajans' precipitation rule, which is evidenced by the low calculated equilibrium precipitation constants [38].

6. Conclusions

This paper provides an empirical construct of the use of thermodynamics and free energy correlations developed using existing laboratory data for calculating surface precipitation constants of radionuclides with hydrous ferric oxide and calcite structure.

High statistical significance of the linear free energy correlations developed for the bulk precipitates indicate that empirically derived surface precipitation constants based on these coefficients are useful quantities where thermodynamic data are not available. Surface precipitation is important to model metal uptake quantitatively from aqueous solutions especially at low concentrations of the cation. The developed model is applicable for the surface precipitation of all trivalent cations with hydrous ferric oxide and calcite structures.

References

[1] W. Runde, Los Alamos Sci. 26 (2000) 392.
[2] K.B. Krauskopf, Chem. Geol. 55 (1986) 323.
[3] T. Stumpf, T. Fanghänel, J. Colloid Interface Sci. 249 (2002) 119.
[4] S.H. Withers, R.E. Peale, A.F. Schulte, G. Brownstein, K.M. Beck, W.P. Hess, R.J. Reeder, Phys. Chem. Minerals 30 (2003) 440.
[5] S.L.S.J. Stipp, T. Christensen, L.Z. Lakshtanov, J.A. Baker, T.E. Waight, Radiochim. Acta 94 (2006) 523.
[6] M.M. Fernandes, T. Stumpf, A. Rabung, T. Bauer, T. Fanghänel, in: Proceedings of Clays in Natural & Engineered Barriers for Radioactive Waste Confinement, Tours, France, March 14–18, 2005.
[7] M. Zavarin, S.K. Roberts, N. Hakem, A.M. Sawvel, A.B. Kersting, Radiochim. Acta 93 (2005) 93.
[8] K.J. Farley, D.A. Dzombak, F.M.M. Morel, J. Colloid Interface Sci. 106 (1985) 226.
[9] D. Dzombak, F.M.M. Morel, Surface Complexation Modeling-Hydrous Ferric Oxide, Wiley, New York, 1990.
[10] G. Sposito, The Surface Chemistry of Soils, Oxford University Press, New York, 1984.
[11] D. Dzombak, F.M.M. Morel, J. Colloid Interface Sci. 112 (1986) 588.
[12] L. Charlet, A. Manceau, J. Colloid Interface Sci. 148 (1992) 443.
[13] K.G. Karthikeyan, H.A. Elliott, J. Colloid Interface Sci. 220 (1999) 88.
[14] R.N.J. Comans, J.J. Middleburg, Geochim. Cosmochim. Acta 51 (1987) 2587.
[15] T. Rabung, T. Stumpf, H. Geckeis, R. Klenze, J.I. Kim, Radiochim. Acta 88 (2000) 711.

[16] M. Zavarin, C.J. Bruton, in: Proceedings of Migration, Incline Village, Nevada, September 26–October 1, 1999.
[17] L.E. Katz, K.F. Hayes, J. Colloid Interface Sci. 170 (1995) 491.
[18] S.N. Towle, J.R. Bargars, G.E. Brown Jr., G.A. Parks, J. Colloid Interface Sci. 187 (1997) 62.
[19] R.T. Ford, K.M. Kemner, P.M. Bertsch, Geochim. Cosmochim. Acta 63 (1) (1999) 39.
[20] D.A. Sverjensky, P.A. Molling, Nature 356 (1992) 231.
[21] P.R. Wells, Linear Free Energy Relationships, Academic Press, London, 1968.
[22] O. Exner, Correlation Analysis of Chemical Data, Plenum, New York, 1988.
[23] H. Xu, Y. Wang, J. Nucl. Mater. 275 (1999) 211.
[24] H. Xu, Y. Wang, J. Nucl. Mater. 275 (1999) 216.
[25] H. Xu, Y. Wang, Radiochim. Acta 87 (1999) 37.
[26] H. Xu, Y. Ewang, L. Barton, J. Nucl. Mater. 273 (1999) 343.
[27] Y. Wang, H. Xu, in: Materials Research Society Symposium Proceedings, Scientific Basis for Nuclear Waste Management, vol. 23, 2000, p. 367.
[28] Y. Wang, H. Xu, Geochim. Chosmochim. Acta 65 (2001) 1529.
[29] R.D. Shannon, Acta Crystallogr. A 32 (1976) 751.
[30] D.A. Sverjensky, Nature 358 (1992) 310.
[31] W.M. Murphy, H.C. Helgeson, Geochim. Cosmochim. Acta 51 (1987) 3137.
[32] W.H. Casey, H. Westrich, Nature 355 (1992) 157.
[33] C. Zhu, Chem. Geol. 188 (2002) 23.
[34] C. Zhu, D.A. Sverjensky, Geochim. Cosmochim. Acta 56 (1992) 3435.
[35] J. Ganguly, S.K. Saxene, Mixtures of Mineral Reactions, Springer Verlag, Berlin, New York, 1987. p. 291.
[36] E.L. Shock, H.C. Helgeson, Geochim. Cosmochim. Acta 52 (1988) 2009.
[37] D.G. Brookins, Eh-pH Diagrams for Geochemistry, Springer, Berlin, 1988.
[38] E. Curti, Appl. Geochem. 14 (1999) 433.
[39] R.B. Lorens, Geochim. Cosmochim. Acta 45 (1981) 553.
[40] D. Bosbach, M. Marques, T. Stumpf, K. Dardenne, T. Fanghänel, Geophys. Res. Abstracts 8 (2006) 07416.